Supporting Information

Interface effect of MOF-derived Pr_6O_{11}/SnO_2 composite material enhances oxygen vacancies for achieving highly sensitive detection of *n*-butanol gas

Leilei Zhang, Fubo Gu, Zhihua Wang**

State Key Laboratory of Chemical Resources Engineering, Beijing University of Chemical Technology, Beijing 100029, China

Experiment reagent

$SnCl_2 \cdot 2H_2O$ (98%) and 2-methylimidazole ($C_4H_6N_2$, ≥98%) were purchased from Shanghai Aladdin Bio-Chem Technology Co., Ltd.; $Pr(NO_3)_3 \cdot 6H_2O$ (99%) was obtained from Tianjin Kemaite Chemical Technology Co., Ltd.; Benzene-1,3,5-tricarboxylic acid ($C_9H_6O_6$, 99%) was acquired from Beijing Innochem Technology Co., Ltd.; Ethanol (C_2H_5OH, ≥99.7%) and methanol (CH_3OH, ≥99.5%) were supplied by Tianjin Fuyu Fine Chemical Co., Ltd. All chemical reagents were of analytical grade and were used directly in the experiments.

Testing process of gas sensors

The gas sensing performance of the material was evaluated using a CGS-4TPs (Beijing ELITE TECH Company) gas sensing analysis system. The procedure was as follows: after stabilization of the operating temperature, the chamber cover was closed. A micro-injector was used to withdraw a precise volume of *n*-butanol and inject it into the evaporation dish inside the chamber from the right side. And during selective testing, all liquids are injected from the right injection port. The evaporation temperature was maintained at 180 ℃. Upon injection, *n*-butanol rapidly volatilized and uniformly filled the chamber, where it interacted with the sensor surface. For n-type semiconductors, when detecting reducing gases, the response is expressed as $S = R_a/R_g$; when detecting oxidizing gases, the response is expressed as $S = R_g/R_a$, where R_g denotes the resistance in the target gas and R_a represents the resistance in air. The response time is defined as the time required for the resistance of the sensor to change by 90% after being exposed to the target gas, while the recovery time refers to the time needed for the resistance to recover to 90% of its baseline value after opening the chamber cover. The amount of injected *n*-butanol was calculated according to eqn (S1).

$$V_{\text{liquid}} = \frac{V_0 C_g M}{22.4 \rho w} \times 10^{-1} \quad \text{(S1)}$$

In eqn (S1), V_{liquid} (μL) denotes the volume of the injected liquid; C_g is the target concentration; V_0 represents the volume of the detection chamber, which is 1.8 L; M (g/mol) is the molecular weight of the target gas; ρ (g/mL) refers to the density of the target liquid; and w (wt%) indicates the mass fraction of the target liquid.

Unlike liquid injections, when NO_2 is injected from the left injection port, the injection volume is calculated according to eqn (S2).

$$V_{\text{gas}} = V_0 \times \frac{C_g}{C_i} \quad \text{(S2)}$$

In eqn (S2), V_{gas} (μL) denotes the volume of the injected gas and C_i shows the initial concentration.

When testing the moisture resistance of the materials, the humidity control method is as follows: The steps before injecting the target gas solution are as mentioned above. And then environmental humidity testing is commonly employed at low humidity levels. When testing the performance under high humidity conditions, a humidification device is usually used to assist the testing. The air produced by the air generator will carry water vapor obtained through the evaporation of water into the reaction chamber, thereby increasing the humidity of the test. After the humidity has stabilized, the target gas solution is injected and the test is conducted.

Thermogravimetric of the Sn-MOF and Pr-MOF

From Fig. S1a, it can be found that calcination of Sn-MOF is mainly divided into two stages. The first stage is the loss of H_2O molecules, with a weight loss of approximately 15.8%; the second stage is the thermal decomposition of the organic framework, with a weight loss of up to 34.8%; it

reaches stability at a temperature of 474 ℃, indicating that 500 ℃ calcination of Sn-MOF can completely convert to SnO_2. As shown in Fig. S1b, calcination of Pr-MOF is mainly divided into two stages. The first stage is the loss of H_2O molecules, with a weight loss of approximately 22.1%; the second stage is the thermal decomposition of the organic framework, with a weight loss of up to 39.3%; the curve flattens at 498 ℃, indicating that 500 ℃ calcination of Pr-MOF can completely convert to Pr_6O_{11}.

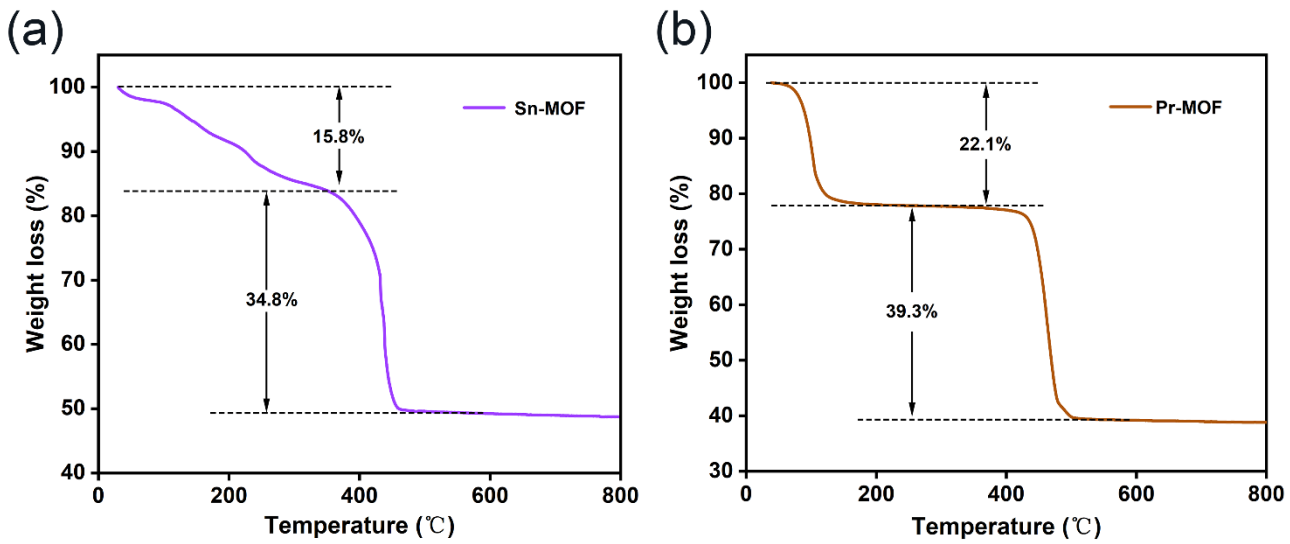

Fig. S1 Thermogravimetric diagram of (a) Sn-MOF and (b) Pr-MOF.

Analysis of crystal structure parameters by XRD

The lattice parameters of SnO_2 were calculated using eqn (S3). Given that SnO_2 possesses a tetragonal crystal structure, the unit cell parameters satisfy $a=b$. The grain size D was calculated using the eqn (S4), while ε was computed according to eqn (S5). The results are summarized in Table S1.

$$\frac{1}{d^2}=\frac{h^2+k^2}{a^2}+\frac{l^2}{c^2} \quad \text{(S3)}$$

$$D=\frac{\sigma\lambda}{\beta\cos\theta} \quad \text{(S4)}$$

$$\varepsilon = \frac{\beta}{4\tan\theta} \quad \text{(S5)}$$

In the equation, h, k, and l denote the Miller indices of the crystal plane; a, b, and c represent the lattice parameters; d is the lattice distance; σ is the Scherrer constant (k = 0.89); λ is the X-ray wavelength (0.154 nm); β is the full width at half maximum of the diffraction peak; and θ is the diffraction angle.

Table S1. Crystal structure parameters of SnO_2 and samples of Pr_6O_{11}/SnO_2 at different ratios.

Sample	Lattice parameter		$d_{(110)}$	D (Å)	ε (%)
	a=b (Å)	c (Å)	(nm)		
SnO_2	0.4732	0.3174	0.3349	62.61	1.87
3 at% Pr_6O_{11}/SnO_2	0.4732	0.3174	0.3343	64.07	1.83
6 at% Pr_6O_{11}/SnO_2	0.4736	0.3173	0.3353	65.24	1.80
9 at% Pr_6O_{11}/SnO_2	0.4736	0.3173	0.3349	63.38	1.84

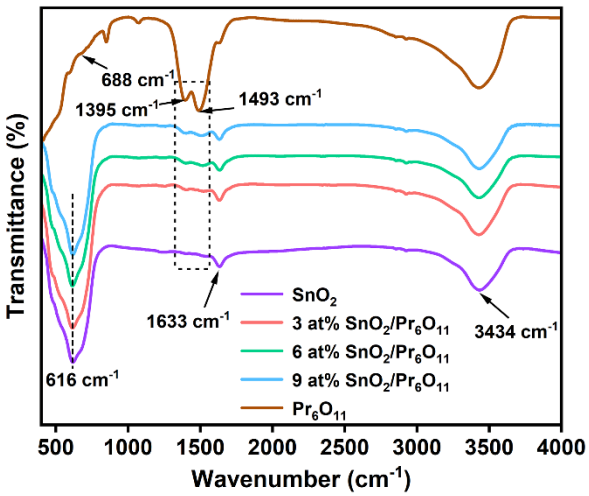

Fig. S2 FTIR spectra of SnO_2, Pr_6O_{11}, and Pr_6O_{11}/SnO_2 sensors with different ratios.

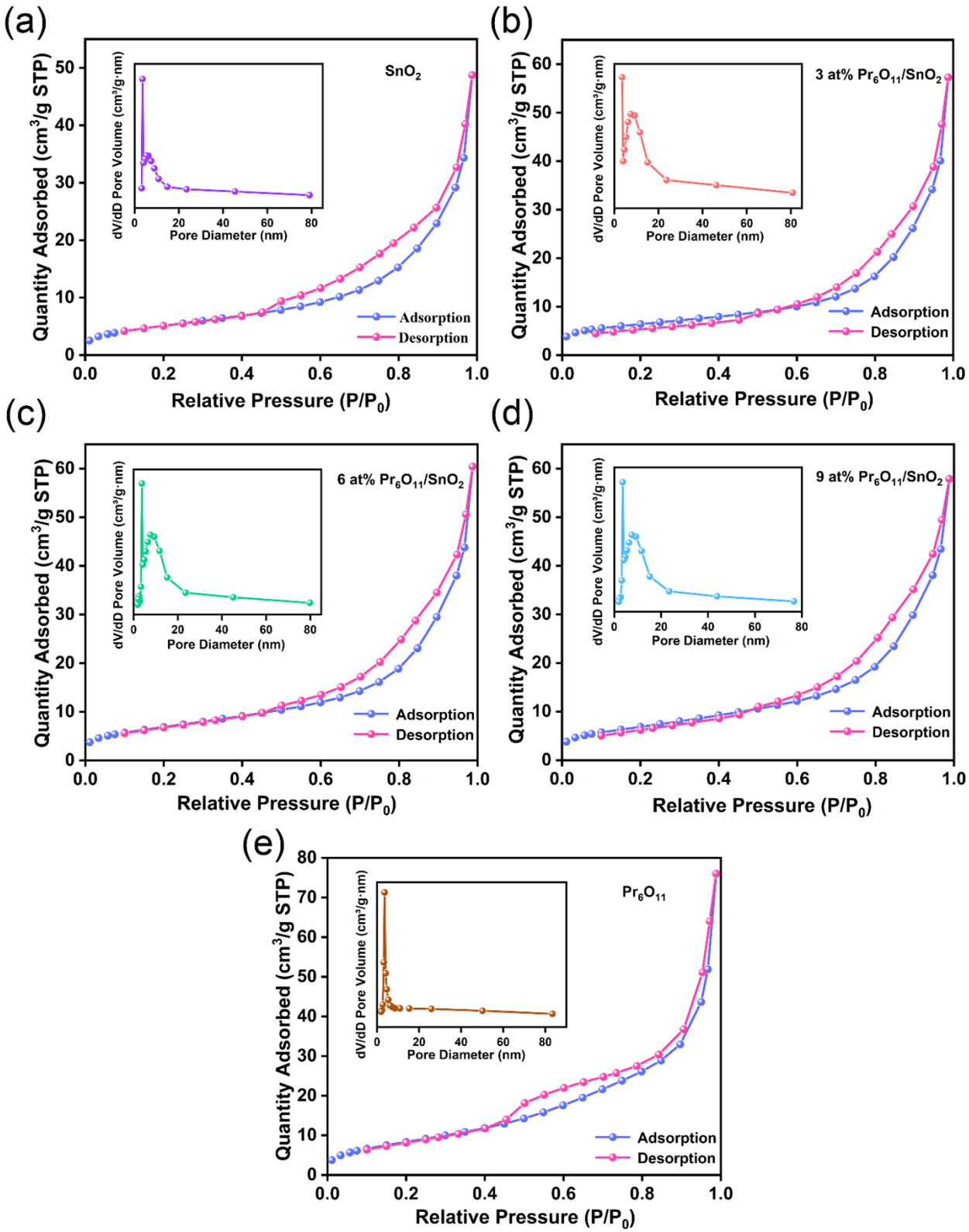

Fig. S3 N_2 isothermal adsorption-desorption curves and pore size distribution: (a) SnO_2; (b) 3 at% Pr_6O_{11}/SnO_2; (c) 6 at% Pr_6O_{11}/SnO_2; (d) 9 at% Pr_6O_{11}/SnO_2; (e) Pr_6O_{11} (The insets are the pore size distribution of samples).

Table S2. Surface area and pore size information of SnO_2, Pr_6O_{11}, and Pr_6O_{11}/SnO_2 sensors.

Samples	Surface area (m^2/g)	Pore size (nm)
SnO_2	19.00	11.86
3 at% Pr_6O_{11}/SnO_2	22.54	12.81
6 at% Pr_6O_{11}/SnO_2	25.17	16.10
9 at% Pr_6O_{11}/SnO_2	25.10	14.05
Pr_6O_{11}	32.15	10.66

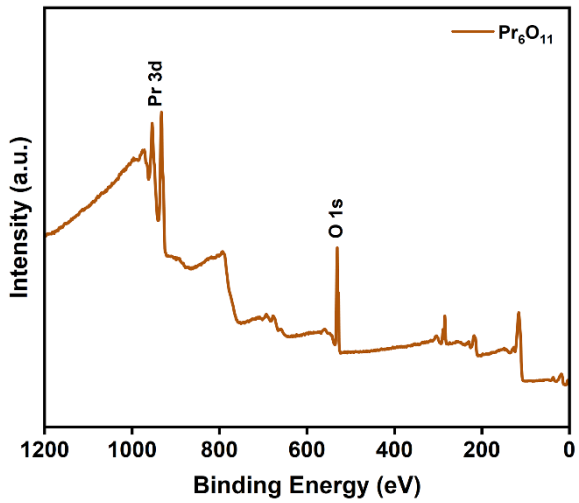

Fig. S4 The full XPS spectrum of Pr_6O_{11}.

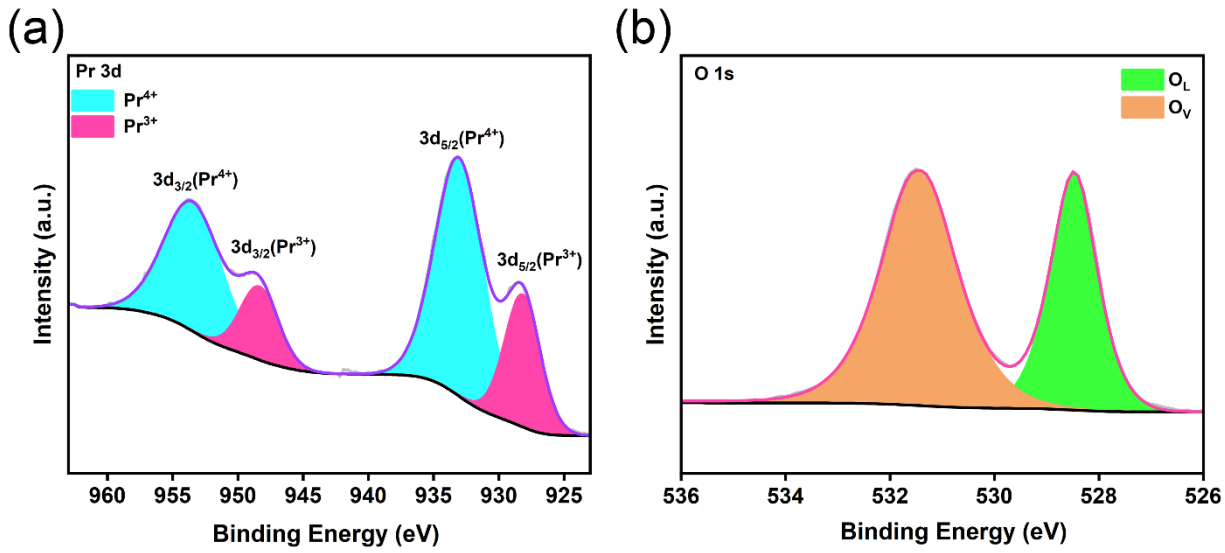

Fig. S5 XPS spectra of Pr_6O_{11}: (a) Pr 3d; (b) O 1s.

Table S3. Atomic percentages of Pr and Sn in Pr_6O_{11}/SnO_2 sensors with different ratios.

Samples	XRF Pr/Sn (at%)	XPS Pr/Sn (at%)	EDS Pr/Sn (at%)
3 at% Pr_6O_{11}/SnO_2	3.60	7.13	7.61
6 at% Pr_6O_{11}/SnO_2	6.75	13.08	10.48
9 at% Pr_6O_{11}/SnO_2	10.75	17.86	12.88

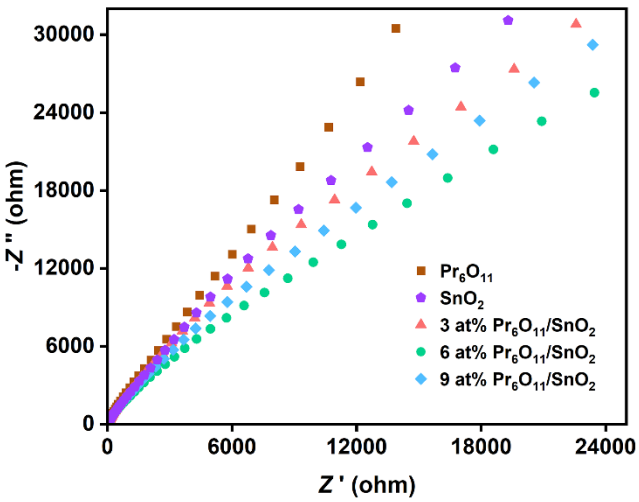

Fig. S6 Nyquist plots of SnO_2, Pr_6O_{11}, and Pr_6O_{11}/SnO_2 samples in different ratios.

Band structure calculation of SnO_2 and Pr_6O_{11}

The sign of the slope of the Mott-Schottky curve can indicate the type of semiconductor. The slope of n-type semiconductor is positive, while that of p-type semiconductor is negative. Thus, it can be determined that both SnO_2 and Pr_6O_{11} are n-type semiconductors. As shown in Fig. S7a and S7c, the valence band potential of SnO_2 is 3.33 eV, and that of Pr_6O_{11} is 0.48 eV. According to eqn (2), the valence band potential of the SnO_2 sample relative to the standard hydrogen electrode (NHE) is 3.24 eV; the valence band potential of the Pr_6O_{11} sample relative to the standard hydrogen electrode is 0.39 eV. Fig. S7b and S7d show the Mott-Schottky diagrams of SnO_2 and Pr_6O_{11} at 500, 1000, and 1500 Hz. It can be obtained that the flat band potentials (E_{FB}) of SnO_2 and Pr_6O_{11} are -0.20 eV and -1.40 eV, respectively, and the flat band potentials relative to the standard hydrogen electrode are 0 eV and -1.20 eV. The potential of the conduction band is 0.1 eV lower than that of the flat band. Therefore, the conduction band potential of SnO_2 relative to the standard hydrogen electrode is -0.10 eV, and that of Pr_6O_{11} is -1.30 eV. Combining eqn (3) and the calculated E_{CB} and E_{VB}, the band gap width of SnO_2 is 3.34 eV, and that of Pr_6O_{11} is 1.69 eV, which is consistent with the UV-vis results.

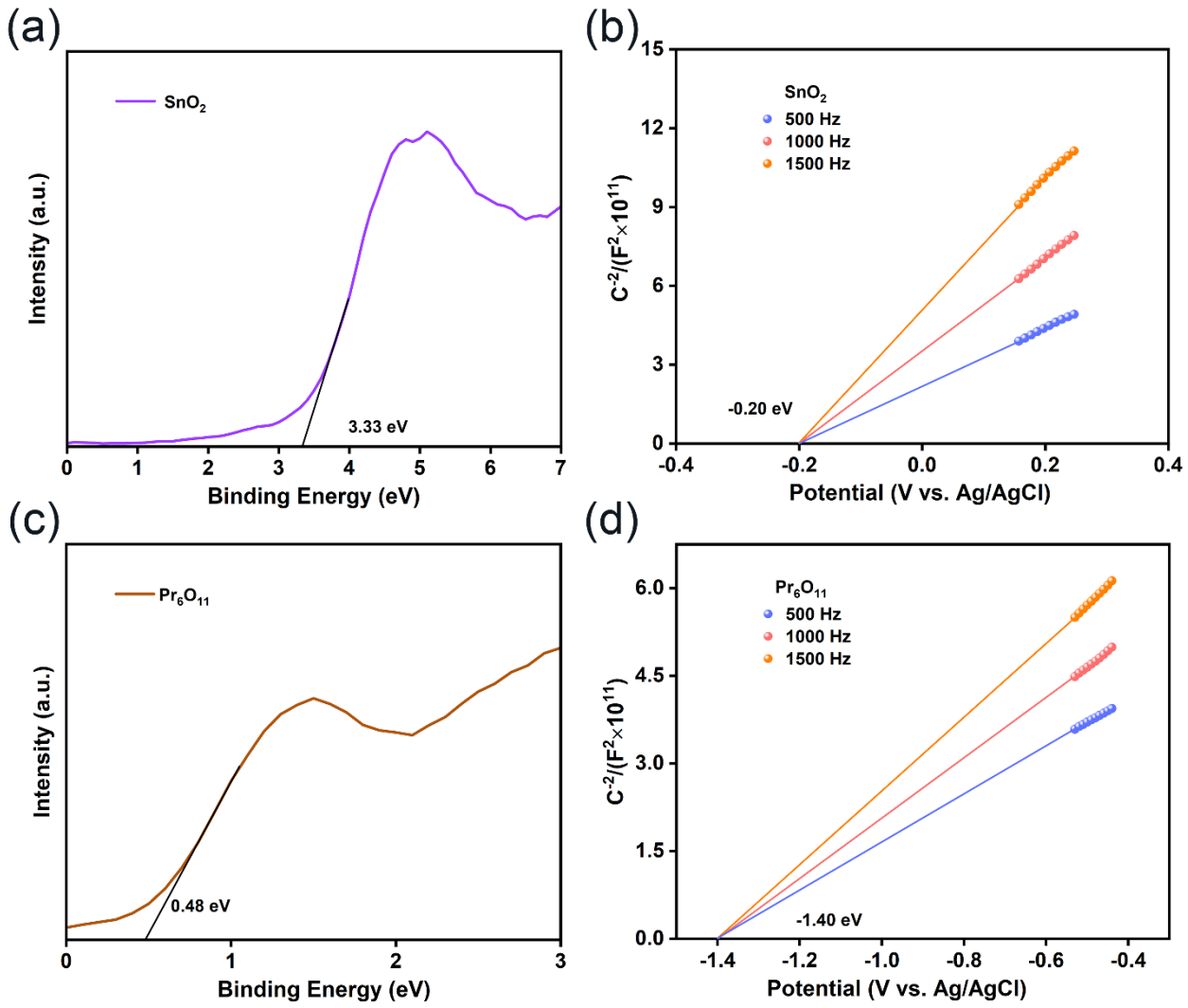

Fig. S7 (a) VB-XPS spectrum of SnO_2; (b) Mott-Schottky plot of SnO_2; (c) VB-XPS spectrum of Pr_6O_{11}; (d) Mott-Schottky plot of Pr_6O_{11}.

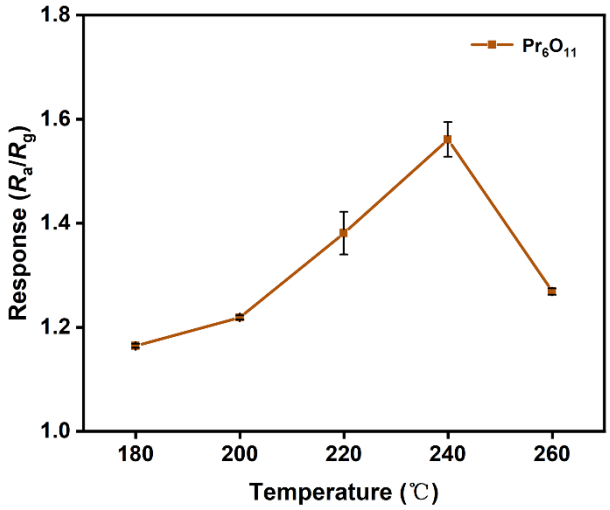

Fig. S8 The response curve of Pr_6O_{11} to 100 ppm *n*-butanol at different temperatures.

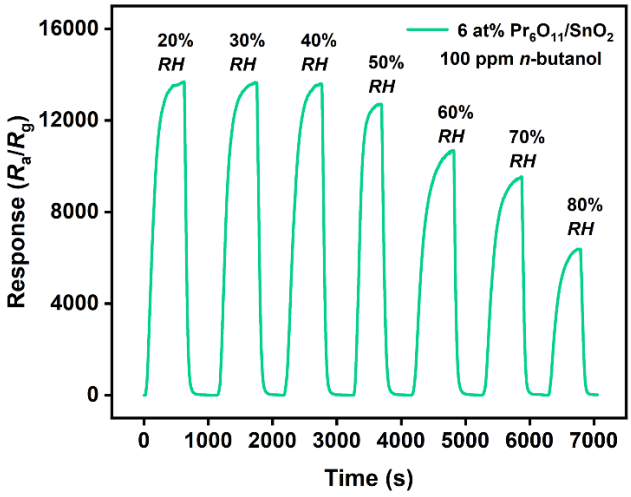

Fig. S9 The real-time response curve of 100 ppm *n*-butanol at different relative humidity at 220 ℃.

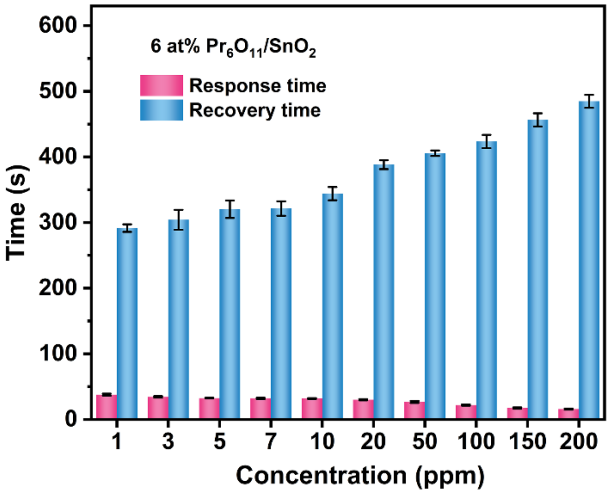

Fig. S10 The response and recovery times of 6 at% Pr_6O_{11}/SnO_2 sensors to different concentrations of *n*-butanol.

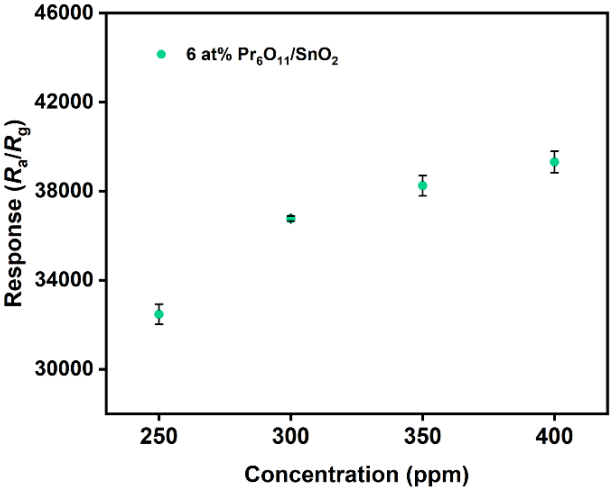

Fig. S11 The response curve of 6 at% Pr_6O_{11}/SnO_2 sensor to 250-400 ppm *n*-butanol gas.

Table S4. Calculation results of theoretical detection limits for SnO_2 and Pr_6O_{11}/SnO_2 composite materials.

Time (s)	SnO_2		3 at% Pr_6O_{11}/SnO_2		6 at% Pr_6O_{11}/SnO_2		9 at% Pr_6O_{11}/SnO_2	
	Y_i-Y	$(Y_i$-$Y)^2$	Y_i-Y	$(Y_i$-$Y)^2$	Y_i-Y	$(Y_i$-$Y)^2$	Y_i-Y	$(Y_i$-$Y)^2$
1	-0.00545	2.97E-5	0.00229	5.25E-6	0.00374	1.40E-5	-0.00505	2.55E-5
19	0.00436	1.90E-5	-0.00311	9.66E-6	-0.00507	2.57E-5	-0.00390	1.52E-5
39	0.00436	1.90E-5	0.00049	2.40E-7	0.00079	6.24E-7	0.00305	9.29E-6
59	-0.00218	4.75E-6	-0.00670	4.49E-5	0.00079	6.24E-7	0.00770	5.93E-5
79	-0.00001	1.00E-10	0.00409	1.68E-5	0.00671	4.50E-5	0.00189	3.56E-6
99	0.00108	1.17E-6	0.00049	2.40E-7	-0.00507	2.57E-5	0.00189	3.56E-6
119	-0.00328	1.08E-5	-0.00311	9.66E-6	-0.00215	4.61E-6	-0.00736	5.42E-5
139	0.00327	1.07E-5	0.00409	1.68E-5	-0.00215	4.61E-6	-0.00390	1.52E-5
159	-0.00110	1.21E-6	0.00229	5.25E-6	0.00374	1.40E-5	0.00654	4.27E-5
179	-0.00437	1.91E-5	-0.00311	9.66E-6	0.00079	6.24E-7	0.00305	9.29E-6
199	0.00327	1.07E-5	0.00229	5.25E-6	-0.00215	4.61E-6	-0.00390	1.52E-5
δ	2.886		29.97		130.1		86.31	
LOD (ppb)	3.690		0.3524		0.08624		0.1748	

$$RMS = \sqrt{\frac{\sum (Y_i - Y)^2}{N - 1}} \quad \text{(S6)}$$

$$LOD(\text{ppb}) = \frac{3RMS}{\delta} \times 1000 \quad \text{(S7)}$$

In the equation, Y_i denotes the actual response at the baseline, N represents the number of

sampling points on the baseline, Y is the average response of the N measurement points, and δ refers to the sensor sensitivity.

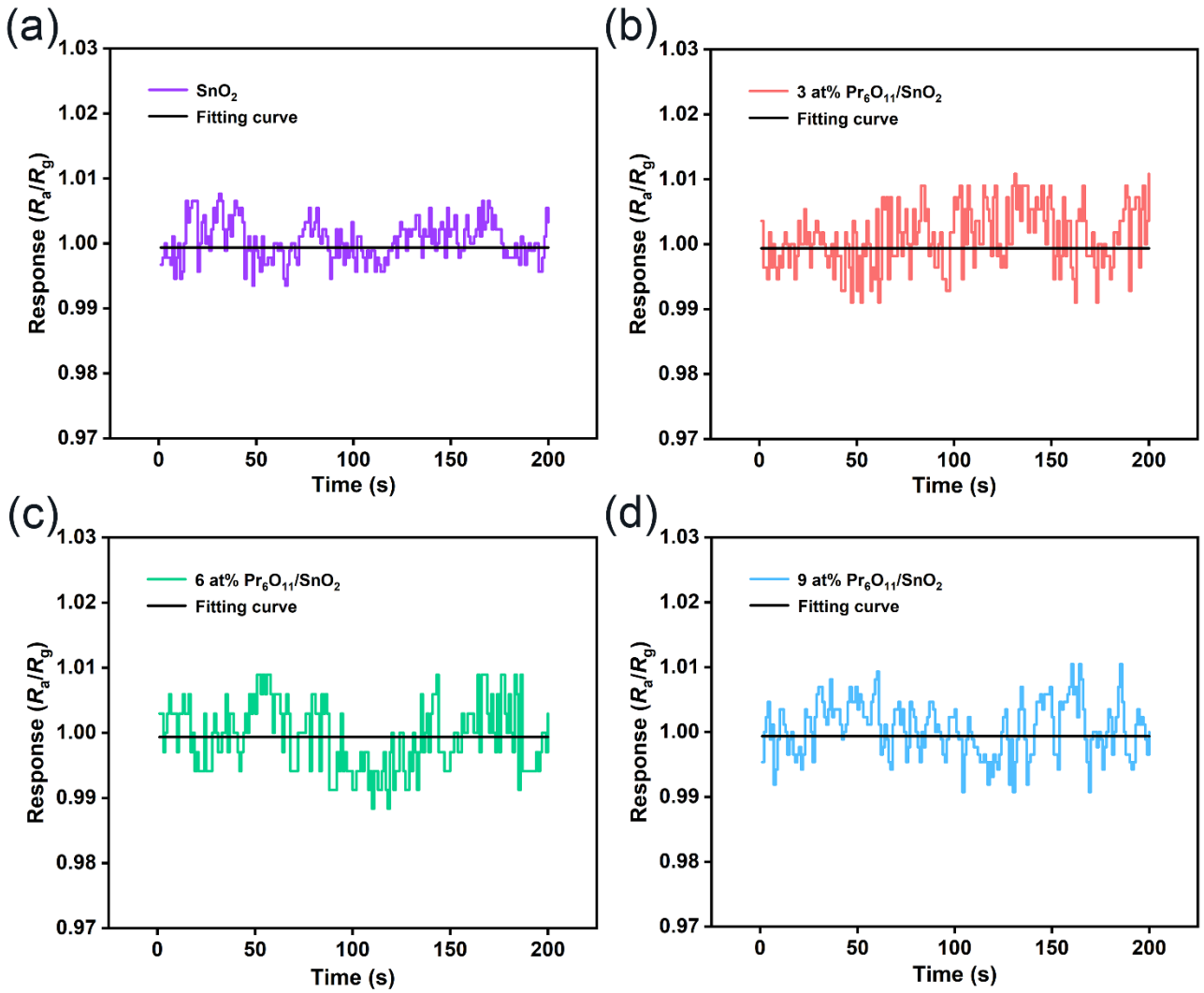

Fig. S12 Baseline of four sensors exposed to *n*-butanol gas: (a) SnO_2; (b) 3 at% Pr_6O_{11}/SnO_2; (c) 6 at% Pr_6O_{11}/SnO_2; (d) 9 at% Pr_6O_{11}/SnO_2.